T.&A.M REPORT NO. 275

CRACK EXTENSION IN FIBERGLASS REINFORCED PLASTICS

by

Edward M. Wu
R. C. Rauter, Jr.

Sponsored by

U. S. Bureau of Naval Weapons
Contract NOw 64-0178-d

DEPARTMENT OF THEORETICAL AND APPLIED MECHANICS
UNIVERSITY OF ILLINOIS

T&AM Report No. 275

CRACK EXTENSION IN FIBERGLASS REINFORCED PLASTICS

by

Edward M. Wu and R. C. Reuter, Jr.

Sponsored by

U. S. Bureau of Naval Weapons
Contract NOw 64-0178-d

Department of Theoretical and Applied Mechanics

University of Illinois
Urbana, Illinois

February 1965

ACKNOWLEDGMENT

This investigation was part of the work in the study of factors controlling the strength of composite structures sponsored by the Navy Bureau of Weapons, Contracts NOw 64-0178-d and NOw 65-0204-d. This investigation was conducted at the University of Illinois in the Department of Theoretical and Applied Mechanics of which Professor T. J. Dolan in Head.

Special acknowledgment is due to Professor H. T. Corten for his helpful criticism and suggestions.

The authors are indebted to Jeff Riggs for rendering valuable assistance in carrying out the experiments, Charles McNabb for preparing the drawings, and Mrs. H. Corray for preparing the manuscript.

TABLE OF CONTENTS

BLANK PAGE

I. INTRODUCTION

Recently, composite materials have received increasing use in aerospace applications due to their superior strength-to-weight ratios. However, as with all structural materials, flaws are unavoidable and a knowledge of fracture behavior of the composites is required. Crack extension in orthotropic parallel filament composite material is considered in this report.

The application of fracture mechanics to orthotropic plates containing a crack was previously examined[1]*. It was observed that the crack tip stress singularity was of the order, $r^{-1/2}$, and stress intensity factors, $k_1 = \sigma\sqrt{a}$ and $k_2 = \tau\sqrt{a}$, similar to those used in isotropic materials were found to be applicable. Observations of crack extension in combined tension and shear experiments performed on balsa wood plates containing a crack verified the fact that for each combination of loading, k_1 and k_2 were constant. Furthermore, the existance of a functional relation between k_1 and k_2 was proposed.

If the above observations and proposal were correct, they should be applicable to other orthotropic materials as well. The experimental investigation described in this report was performed on fiberglass reinforced plastics to provide such verification. Also, attention has been given to a physically meaningful definition of crack stability in order that the test results can be evaluated under a consistent criterion.

This experimental investigation was conceived in search of a general fracture criterion which is applicable to all orthotropic materials. Several possibilities are examined and areas where further investigation is needed are noted.

II. PURPOSE

The purpose of the experimental program was three fold: First, to examine whether the fracture strengths of orthotropic fiberglass reinforced plastic conform to the laws of linear-elastic fracture mechanics, second, to observe the mode of crack extension in orthotropic plates, and third, to compare the above results with previous findings [1] on balse wood plates and investigate the possible existence of general fracture criterion applicable to all statistically homogeneous orthotropic materials.

III. EXPERIMENTAL INVESTIGATION

A. Experimental Set-Up

Cured plastic sheets 0.05 inch thick reinforced with unidirectional non-woven

---

* Numbers in brackets designate References listed.

fiberglass filaments (Scotchply type 1002 made by Minnesota Mining and Manufacturing Co.) were selected as specimen material for this experimental investigation. These plates were cut into specimens. A slot was introduced into each specimen using a fine jeweler's saw along the direction of glass fiber reinforcement. The tips of the saw slot were wedged open slightly using a sharp razor blade in order to simulate a natural crack. The dimensions of the plates were chosen such that the length was sufficiently long to prevent the crack from propagating into the grips and the ratio of the plate width (at the line of the crack) to the crack length was sufficiently large to minimize the edge effect of the plate. The dimensions and crack lengths of the specimens are listed in Table 1.

Specimens thus prepared were tested under three types of loading conditions:

1) Tension perpendicular to the crack - the case of symmetric loading with respect to the crack.
2) Combined tension and shear - the case of combined symmetric and skew-symmetric loadings.
3) Pure shear - the case of skew-symmetric loading.

These tests were all performed in an Instron testing machine where the above loading conditions were achieved by special arrangements.

For tension loading, the specimens were secured in grips between rubber shims and pulled perpendicular to the crack, Fig. 1.

For combined tension and shear loadings, a similar method of gripping was used while the ratio of tension force (perpendicular to the crack) to shearing force was controlled by orientating the direction of the crack (hence, the direction of the fiber-glass reinforcement)at an angle γ to the direction of the tension load, Fig. 2.

For pure shear, a rig was designed to load a cantilever beam type of specimen in the plane of the plate as illustrated in the schematic drawing and photograph of the apparatus, Fig. 3 and 4. Thus, a state of pure shear stress was achieved at the crack tips located along the neutral axis of the beam specimen. To prevent this narrow beam specimen from buckling, two Teflon lined plexiglas plastic side plates were used to constrain it to bend in plane.

During the tests, the loads were recorded on the Instron load-time chart while the crack lengths were recorded by a motor-driven 35 mm camera. To facilate the crack observation and recording, a solution of ethylene glycol and black India ink was

introduced into the crack. Alternately, in the combined tension and shear tests, the crack could be made visible by adjusting the incident angle of a light beam shining on it. This alternate method of crack observation offered a means of comparing the respective strengths of the specimens during the presence and absence of the marking ink solution. To the degree of experimentally accuracy, the effect of the ink on the fracture strengths of the specimens was negligible.

A small grid of known dimensions was glued close to the crack in order to provide a scale factor when the cracks were measured by projecting the film to approximately 10X magnification. With this system, measurements of the crack accurate to 0.005 inch were easily obtained.

The loading rates for each series of tests were adjusted so as to keep the total time to fracture for each specimen approximately the same. The effect of the loading rate on the fracture strength of the specimens will be discussed in a later section. Data collected in this manner for each specimen were plotted on graphs of stress versus half crack length. Samples of these data are shown in Figs. 5, 6 and 7.

B. Interpretation of Data and Results

From the stress versus crack length data, (Fig. 5, 6 and 7) it is clear that several patterns of crack extension were observed. Some specimens exhibited extensive slow growth while others showed little slow crack growth prior to fracture. In order to compute the critical stress intensity factors, k_1 and k_2, a consiste criterion was required to determine the critical crack length and the corresponding critical stress level. To achieve this end, a criterion based on the premise that a particular rate of crack propagation represents the instability of a cracked plate was used.

During a test, photographs of the crack were taken at decreasing load intervals as the specimen approached fracture. The crack lengths as recorded by the photographs were then plotted against time as recorded by the Instron time-drive chart. Typical samples of these data are shown in Fig. 8. The slope of this crack extension-time curve represents the magnitude of the average velocity of crack propagation during the time interval between photographs. The critical crack length can be determined by defining the critical crack velocity above which the specimens become unstable and fracture abruptly.

This method would provide a consistent criterion for determining the critical

crack length and also the corresponding critical stress if the shape and characteristics of these crack displacement-time curves were of similar form regardless of whether the crack was extended by symmetric or skew-symmetric external stresses. Unfortunately, this was not the case. The crack displacement curves for all specimens separated into three basic types. Further it was found that the type of crack displacement curve appeared to be related to the state of stress. The first type of curve exhibited a gradual increase in average crack velocity as the external load was increased (curves denoted by Δ , Fig. 8) indicating possibly that the crack extended into a uniform region of material. The second type of curve showed a smaller increase in crack velocity as the external load was increased followed by an abrupt increase in velocity which led to fracture (curves denoted by $\square$, Fig. 8). This may indicate that the crack propagated from a strong region into a weaker region causing the sudden increase in crack velocity. The third type of curve exhibited a series of large abrupt increments of crack extension and arrest which commenced at stress levels well below the critical stress. This pattern frequently was repeated several times resulting in a step-shaped curve (curves denoted by O, Fig. 8). A possible explantion for this pattern is that although the fractured specimen appeared to be separated in the direction of the glass fiber reinforcement along essentially a straight line, the crack may have skipped across fibers on a microscopic scale. This phenomena could explain the intermittent high resistance to the crack extension. This fiber-crack configuration is shown schematically in Fig. 9 and substantiated by photographs of a magnified crack, Fig. 10, and of several broken specimens, Fig. 11. Also the fact that the crack tips were not always well defined in the photographs lends support to this view, Fig. 10.

As noted earlier, an influence of the state of externally applied stress on the crack propagation pattern was also observed. In general, the amount of slow crack extension and the average crack velocity prior to abrupt fracture (type I pattern) was greater for specimens subjected to symmetric loading (tension) than for those subjected to skew-symmetric (shear) loading. Moreover, the type III step-shaped crack extension pattern occurred more frequently when the ratio of (shear load)/(tension load) was increased. This is indicated in Table 1 where the frequency of large abrupt crack extension and arrest per specimen is compared to the ratio of externally applied (shear/tension)stress.

Despite these differences in crack extension patterns the critical crack lengths determined from the crack displacement-time curves by using this critical velocity concept provided better consistency than other criteria tried while at the same time

offered a meaningful physical interpretation as well. By comparing curves with a well defined abrupt change in slope, a small range of crack velocity above which the specimen fractured abruptly was chosen as the critical crack velocity. With this range of critical velocities, the critical crack lengths for other specimens whose crack extension curves did not have a well defined transition were determined. Critical crack lengths determined in this manner were then used to determine the critical stresses (σ or τ or both, which ever applies) from the stress versus crack length graphs (Figs. 5, 6 and 7).

The results for specimens subjected to pure tension and pure shear are shown in diagrams with log σ as ordinate and, a (half crack length) as abscissa in Fig. 12 and 13. The result of one group of combined tension and shear, at the ratio $\tau/\sigma = 2.14$, is shown in Fig. 14 and 15.

The stress intensity factors for all the specimens tested were computed from the relations.

$$k_1 = \sigma\sqrt{a},$$

and

$$k_2 = \tau\sqrt{a}.$$

Values of k_1 and k_2 for all specimens are tabulated in Table 1, and plotted in Fig. 16. Also listed in Table 1 is the approximate time to fracture for every specimen. It should be noted that in the pure tension test, two groups of specimens were tested where the loading rates were changed so that the time to fracture for the second group is about 3 times longer than that of the first group. No significant difference between the average k_1 values for the two groups could be detected. Since the time to fracture for all of the tests were well within this limit, the effect of the loading rate effect can be neglected.

IV. DISCUSSION OF RESULTS

The elastic constants for the Scotch-ply specimens, measured according to the method suggested by S. W. Tsai [2], are

$$a_{11} = 0.20 \times 10^{-6} \qquad a_{12} = -0.01 \times 10^{-6}$$

$$a_{22} = 0.60 \times 10^{-6} \qquad a_{66} = 1.42 \times 10^{-6}$$

With these values, the auxiliary equation of the partial differential equation for the stress function

$$\frac{\partial^4 U}{\partial x^4} + \left(\frac{2a_{12} + a_{66}}{a_{22}}\right) \frac{\partial^4 U}{\partial x^2 \partial y^2} + \frac{a_{11}}{a_{22}} \frac{\partial^4 U}{\partial y^4} = 0 \qquad (1)$$

has four pure imaginary roots and they are

$$s_1 = i\beta_1 = i\,2.53 \qquad s_2 = i\beta_2 = i\,0.68$$

$$\bar{s}_1 = -i\beta_1 = -i\,2.53 \qquad \bar{s}_2 = -i\beta_2 = -i\,0.68$$

Previous discussion on the solution of equation (1) for an infinite plate containing a single crack[1] is applicable to this case. With proper adjustment for the case of four imaginary roots instead of four complex roots of equal absolute magnitude, the crack tip stress distributions are:

$$\sigma_x = \frac{\sigma\sqrt{a}}{\sqrt{2r}} \frac{\beta_2\beta_1}{(\beta_2-\beta_1)} \left\{ \frac{\beta_2 \cos\frac{\phi_2}{2}}{(\cos^2\theta + \beta_2^2 \sin^2\theta)^{1/4}} - \frac{\beta_1 \cos\frac{\phi_1}{2}}{(\cos^2\theta + \beta_1^2 \sin^2\theta)^{1/4}} \right\}$$

$$+ \frac{\tau\sqrt{a}}{\sqrt{2r}} \frac{1}{(\beta_2-\beta_1)} \left\{ \frac{\beta_1^2 \sin\frac{\phi_1}{2}}{(\cos^2\theta + \beta_1^2 \sin^2\theta)^{1/4}} - \frac{\beta_2^2 \sin\frac{\phi_2}{2}}{(\cos^2\theta + \beta_2^2 \sin^2\theta)^{1/4}} \right\}$$

$$\sigma_y = \frac{\sigma\sqrt{a}}{\sqrt{2r}} \frac{1}{(\beta_2-\beta_1)} \left\{ \frac{\beta_2 \cos\frac{\phi_1}{2}}{(\cos^2\theta + \beta_1^2 \sin^2\theta)^{1/4}} - \frac{\beta_1 \cos\frac{\phi_2}{2}}{(\cos^2\theta + \beta_2^2 \sin^2\theta)^{1/4}} \right\}$$

$$+ \frac{\tau\sqrt{a}}{\sqrt{2r}} \frac{1}{(\beta_2-\beta_1)} \left\{ \frac{\sin\frac{\phi_2}{2}}{(\cos^2\theta + \beta_2^2 \sin^2\theta)^{1/4}} - \frac{\sin\frac{\phi_1}{2}}{(\cos^2\theta + \beta_1^2 \sin^2\theta)^{1/4}} \right\} \qquad (2)$$

$$\tau_{xy} = \frac{\sigma\sqrt{a}}{\sqrt{2r}} \frac{\beta_1\beta_2}{(\beta_2-\beta_1)} \left\{ \frac{\sin\frac{\phi_1}{2}}{(\cos^2\theta + \beta_1^2 \sin^2\theta)^{1/4}} - \frac{\sin\frac{\phi_2}{2}}{(\cos^2\theta + \beta_2^2 \sin^2\theta)^{1/4}} \right\}$$

$$+ \frac{\tau\sqrt{a}}{\sqrt{2r}} \frac{1}{(\beta_2-\beta_1)} \left\{ \frac{\beta_2 \cos\frac{\phi_2}{2}}{(\cos^2\phi + \beta_2^2 \sin^2\phi)} - \frac{\beta_1 \cos\frac{\phi_1}{2}}{(\cos^2\theta + \beta_1^2 \sin^2\theta)^{1/4}} \right\}$$

where

$$\sin\phi_1 = \frac{\beta_1 \sin\theta}{(\cos^2\theta + \beta_1^2 \sin^2\theta)^{1/2}} \quad ; \quad \sin\phi_2 = \frac{\beta_2 \sin\theta}{(\cos^2\theta + \beta_2^2 \sin^2\theta)^{1/2}}$$

$$\cos\phi_1 = \frac{\cos\theta}{(\cos^2\theta + \beta_1^2 \sin^2\theta)^{1/2}} \quad ; \quad \cos\phi_2 = \frac{\cos\theta}{(\cos^2\theta + \beta_2^2 \sin^2\theta)^{1/2}} \tag{3}$$

It was found in the previous investigations on balsa wood that the stress intensity factors $k_1 = \sigma\sqrt{a}$, $k_2 = \tau\sqrt{a}$ which were separable from the crack tip stress distribution equations (2), could be used as parameters to characterize the size of the crack and the magnitude of external stresses. Furthermore k_{1c} and k_{2c} were constant for balsa wood. As it is evident from the results of the experimental investigation here, the stress intensity factors for Scotchply are also constants when it was subjected to tension (Fig. 12), shear (Fig. 13) and combined tension and shear (Fig. 14 and 15).

In order to consider the criterion which relates k_{1c} and k_{2c} in a functional relationship (represented by the experimental results in Fig. 16) a clear idea of the mode of crack extension is required. From the experimental observations two possibilities exist:

A. The crack propagates in a straight line colinear with the original and along the glass fiber reinforcements.

B. The crack propagates along an essentially straight line but makes microscopic skips across neighboring glass fibers.

Possible fracture criteria which are applicable to the two modes shall be discussed separately.

A. If the first mode is correct, then only the stress distributions co-linear with the original crack need to be considered since this is the location of crack propagation. Therefore for $\theta = 0$ $\phi = 0$ Eq. (2) becomes

$$\sigma_x = \frac{\sigma\sqrt{a}}{\sqrt{2r}}\beta_2\beta_1$$

$$\sigma_y = \frac{\sigma\sqrt{a}}{\sqrt{2r}} \tag{4}$$

$$\tau_{xy} = \frac{\tau\sqrt{a}}{\sqrt{2r}}$$

In order to examine the possibility of using a maximum stress criterion, some modification to the common expressions for maximum normal stress and maximum shear stress is needed since at the tip of the crack where $r \to 0$, $\sigma_y \to \infty$ and $\tau_{xy} \to \infty$. However, this difficulty can be avoided by considering

$$\sigma_y \sqrt{2r} = \text{constant} \tag{5}$$

$$\tau_{xy} \sqrt{2r} = \text{constant} \tag{6}$$

as maximum stress type of criteria for crack extension. From Eq. 4 it can be deduced that neither a maximum normal stress type of criterion, Eq. 5 nor a maximum shear type of criterion, Eq. 6 can fully describe the fracture phenomenon of this orthotropic plate. This follows by considering the case where specimens fractured under pure tension, i.e. $\tau = 0$. The absence of shearing stress ($\tau_{xy} = 0$) eliminates the possibility of using Eq. 5 as a criterion. On the other hand in the case of fracture under pure shear, where $\sigma = 0$ then $\sigma_y = 0$, in turn eliminates the possibility of using Eq. 5 as a criterion since a correct criterion must encompass both of these cases. A maximum energy release rate also has been suggested as a possible criterion [3, 4], i.e.

$$\mathcal{G}_I + \mathcal{G}_{II} = \text{Constant} \tag{7}$$

where the quantities $\mathcal{G}_I$ and $\mathcal{G}_{II}$ are given by [5]

$$\mathcal{G}_I = \pi k_1^2 \sqrt{\frac{a_{22}a_{11}}{2}} \left(\sqrt{\frac{a_{22}}{a_{11}}} + \frac{a_{66} + 2a_{12}}{2a_{11}} \right)^{1/2} \tag{8}$$

$$\mathcal{G}_{II} = \pi k_2^2 \frac{a_{11}}{\sqrt{2}} \left(\sqrt{\frac{a_{22}}{a_{11}}} + \frac{a_{66} + 2a_{12}}{2a_{11}} \right)^{1/2}$$

Substitution of Eq. (8) into Eq. (7) leads to

$$k_1^2 + \sqrt{\frac{a_{11}}{a_{22}}}\, k_2^2 = \text{constant} \tag{9}$$

If Eq. (7) is true then Eq. (9) must hold for both of the following conditions:

$$\begin{aligned} &\text{pure tension: } k_1 = k_{1c} \qquad k_2 = 0 \\ &\text{pure shear: } k_1 = 0 \qquad k_2 = k_{2c} \end{aligned} \tag{10}$$

By substituting Eq. (10) in Eq. (9), the following relationship is obtained:

$$\left(\frac{k_{1c}}{k_{2c}}\right)^4 = \frac{a_{11}}{a_{22}}$$

For Scotch-ply:

$$\left(\frac{k_{1c}}{k_{2c}}\right)^4 = \left(\frac{930}{3580}\right)^4 = 0.0045$$

and

$$\frac{a_{11}}{a_{22}} = \frac{0.20 \times 10^{-6}}{0.60 \times 10^{-6}} = 0.35$$

It can be seen that these two values differ by almost 2 orders of magnitude and Eq. 11 is not satisfied. Equation (9) is also represented in Fig. 16. There is little doubt that if the crack propagates straight ahead, i.e. co-linearly with the original crack, constant maximum energy release rate, Eq. 7, is not a realistic criterion.

B. If the second suggested mode of crack extension occurs, i.e. the crack skips across fibers, then the possibility of using maximum stress criteria, Eq. 5, 6, or maximum energy release rate, Eq. 7, can no longer be eliminated.

In order to examine the applicability of Eq. 5 or Eq. 6, $\sigma_y\sqrt{2r}$ or $\tau_{xy}\sqrt{2r}$ respectively must be maximized and the angle θ_{max} at which they occur must be calculated and compared to the actual observations of the crack extension pattern. The curves which represent these criteria can then be compared to the experimentally determined relationship between k_1 and k_2 in Fig. 16. However, it is very difficult to obtain an explicit representation for θ in terms of $\sigma_y\sqrt{2r}$ and $\tau_{xy}\sqrt{2r}$. Investigation along these lines together with more detailed observations of the crack extension modes will be carried out in the future.

In order to examine the possibility of using maximum energy release rate as a criterion for the second mode of crack extension, the elastic energy release rate for a configuration as indicated in Fig. 9 must be calculated. The authors know of no such mathematical solution available and suggest this phase warrants further investigation.

Since at present a suitable fracture criterion can not yet be developed, its representation in the form of an empirical equation shall be presented. When results are plotted in a graph of dimensionless quantities k_1/k_{1c} versus k_2/k_{2c} (Fig. 18) it

can be noted that the empirical relation:

$$\left(\frac{k_1}{k_{1c}}\right) + \left(\frac{k_2}{k_{2c}}\right)^2 = 1$$

which was observed to fit the data for balsa wood also fits the data for Scotch-ply equally well. The data for balsa wood is presented again in Fig. 19 for comparison.

The relation

$$\left(\frac{k_1}{k_{1c}}\right)^2 + \left(\frac{k_2}{k_{2c}}\right)^2 = 1$$

which represent the maximum energy release rate (Eq. 7) based on co-linear crack propagation is also shown in these figures.

V. SUMMARY AND CONCLUSIONS

Experimental investigation on initially cracked Scotch-ply plates indicated that the fracture strength of this fiberglass reinforced plastics can be described by the laws of linear elastic fracture mechanics. The stress intensity factors, k_{1c} and k_{2c}, were constants for symmetric and skew-symmetric loadings. Furthermore, k_1 and k_2 were also found to be constants for various combinations of symmetric and skew-symmetric loadings.

As indicated by photographs of the fractured specimens and the crack displacement time curves it was observed that although the cracks propagated along lines which were essentially straight, it is probable that the cracks made microscopic skips across the fiberglass reinforcement in the vicinity of this line in a discontinuous manner as suggested in Fig. 11. This phenomena occurs more frequently when the specimens were subjected to shearing stress.

At present, because the modes of crack extension under different type of loading are not fully understood, and also due to the mathematical difficulties involved in the calculation of maximum normal stress, maximum shear stress and maximum energy release rate, a general law of fracture applicable to all orthotropic materials cannot be formulated without further analytical and experimental investigations.

The empirical equations

$$\left(\frac{k_1}{k_{1c}}\right) + \left(\frac{k_2}{k_{2c}}\right)^2 = 1$$

however, was found to be an adequate representation for balsa wood as well as Scotch-ply and could represent a general fracture law for orthotropic materials.

VI. REFERENCES

1. Wu, E. M.: Application of Fracture Mechanics to Orthotropic Plates, University of Illinois T&AM Report No. 248, 1963.

2. Tsai, S.W.: Experimental Determination of Elastic Behavior of Orthotropic Plates, ASME Paper No. 64-WA/MD-1.

3. Paris, P.C. and G. S. Sir: Stress Analysis of Cracks Lehigh University Institute of Research Report, June, 1964.

4. Mast, P. : Private Communication.

5. Irwin, G. R.: Analytical Aspects of Crack Stress Field Problems, University of Illinois T&AM Report 213, 1962.

TABLE 1

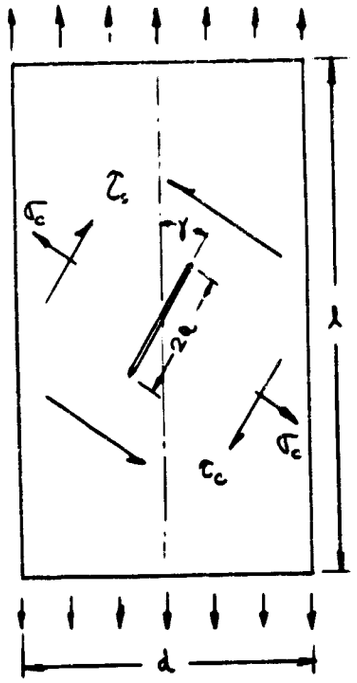

ℓxd - Specimen Dimensions (inches)

a_o - Original Half Crack Length (inches)

a_c - Critical Half Crack Length (inches)

σ_c - Critical Symmetric Stress (psi)

τ_c - Critical Skew-Symmetric Stress (psi)

k_1 - Symmetric Stress Intensity Factor ($lb\text{-}in^{-3/2}$)

k_2 - Skew-Symmetric Stress Intensity Factor ($lb\text{-}in^{-3/2}$)

t - Time to Fracture (min.)

τ_c/σ_c - Average Ratio for Each Group

n - Frequency of Large Abrupt Extension and Arrest of Crack Per Specimen

Spec. No.	ℓxd	a_o	a_c	σ_c	τ_c	k_{1c}	k_2	t	τ_c/σ_c	n
1-90	8x6	0.265	0.325	1830	0	1040	0	4.3		
2-90	"	0.760	0.835	970	0	900	0	6.1		
3-90	"	0.120	0.165	2100	0	850	0	4.6		
4-90	"	0.765	0.840	990	0	910	0	2.9		
6-90	"	0.740	0.765	1070	0	940	0	2.7		
7-90	"	0.745	0.795	970	0	870	0	2.4		
8-90	"	0.270	0.320	1530	0	870	0	3.7		
9-90	"	0.270	0.320	1610	0	910	0	3.8		
10-90	"	0.575	0.635	1230	0	980	0	2.9		
11-90	"	0.510	0.575	1280	0	970	0	3.2		
12-90	"	0.500	0.575	1230	0	930	0	3.3	0	0.27
13-90	"	0.500	0.585	1300	0	1000	0	3.2		
14-90	"	0.115	0.185	2360	0	1010	0	14.2		
15-90	"	0.115	0.160	1960	0	790	0	11.1		
16-90	"	0.165	0.225	1910	0	910	0	11.0		
17-90	"	0.125	0.170	2180	0	900	0	12.5		
18-90	"	0.250	0.320	1650	0	930	0	9.7		
19-90	"	0.265	0.320	1640	0	930	0	10.7		
20-90	"	0.270	0.315	1510	0	850	0	10.2		
21-90	"	0.500	0.610	1260	0	980	0	9.2		
22-90	"	0.502	0.600	1170	0	910	0	8.0		
23-90	"	0.490	0.590	1330	0	1020	0	8.8		

Table 1 continued

Spec. No.	ℓxd	a_o	a_c	σ_c	τ_c	k_1	k_2	t	τ_c/σ_c	n
1-65	8.5x5	0.245	0.275	1600	710	840	370	4.6		
2-65	"	0.510	0.565	1140	510	860	380	3.4		
3-65	"	0.765	0.815	960	410	870	370	2.9		
4-65	"	0.235	0.270	1870	830	970	430	5.5	0.47	0.29
5-65	"	0.475	0.490	1590	610	1110	420	3.9		
7-65	"	0.735	0.760	1150	430	1000	370	3.1		
8-65	"	0.475	0.525	1330	560	960	410	4.1		
1-45	9.5x4	0.255	0.335	1660	1660	960	960	7.3		
2-45	"	0.270	0.320	1640	1630	930	920	7.2		
3-45	"	0.615	0.690	970	970	810	800	3.6		
4-45	"	0.600	0.645	970	970	780	780	4.5		
5-45	"	0.355	0.555	1100	1160	820	870	5.7		
6-45	"	0.485	0.530	1130	1190	820	870	5.9		
7-45	"	0.515	0.580	1110	1000	850	760	5.1	1.00	0.39
8-45	"	0.500	0.560	1090	1110	820	830	5.1		
9-45	"	0.265	0.340	1510	1590	880	930	7.5		
10-45	"	0.245	0.340	1500	1550	870	900	7.1		
11-45	"	0.725	0.775	980	950	860	840	4.7		
12-45	"	0.735	0.780	850	870	750	770	5.0		
13-45	"	0.765	0.780	790	820	700	730	3.9		
14-45	"	0.760	0.840	970	990	890	910	4.4		
2-25	4x12	0.775	0.850	770	1630	710	1500	9.6		
3-25	"	0.985	1.090	760	1580	790	1650	8.8		
4-25	"	0.510	0.615	1030	2060	800	1620	11.9		
5-25	"	0.770	0.915	880	1840	840	1760	10.2		
6-25	"	0.970	1.085	720	1480	750	1550	8.3	2.14	0.40
7-25	"	0.460	0.565	1070	2280	810	1720	13.9		
8-25	"	0.725	0.800	820	1700	730	1520	9.5		
9-25	"	1.015	1.080	720	1530	750	1590	9.5		
10-25	"	0.270	0.340	1380	2900	810	1690	11.0		
11-25	"	0.260	0.290	1380	2950	740	1590	12.5		

Table 1 continued

Spec. No.	ℓxd	a_o	a_c	σ_c	τ_c	k_1	k_2	t	τ_c/σ_c	n
1-20	12x4	0.595	0.745	920	2340	800	2020	9.0		
2-20	"	0.740	0.815	750	1990	670	1800	8.0	2.75	0.50
3-20	"	0.725	0.770	850	2150	740	1890	8.8		
4-20	"	0.400	0.450	1070	2850	720	1910	11.4		
1-15	12x4	0.295	0.355	960	3580	570	2130	14.8		
2-15	"	0.500	0.595	770	2890	600	2230	13.7	3.73	0.50
3-15	"	0.625	0.735	670	2410	570	2060	12.0		
4-15	"	0.270	0.335	1080	2890	620	2250	15.9		
1-12	12x4	0.505	0.610	640	3030	500	2370	13.8		
2-12	"	0.465	0.530	700	3020	510	2200	13.6	4.70	0.75
3-12	"	0.685	0.870	570	2580	530	2410	12.2		
4-12	"	0.715	0.815	620	2790	560	2520	12.7		
1-10	12x4	0.405	0.495	560	3250	390	2290	19.0		
2-10	"	0.795	0.865	470	2760	440	2560	15.6		
3-10	"	0.500	0.590	580	3310	450	2540	17.6		
4-10	"	0.265	0.360	690	3940	420	2360	21.0	5.67	0.43
5-10	"	0.400	0.490	660	3430	390	2400	19.2		
6-10	"	0.490	0.595	610	3520	470	2720	18.8		
7-10	"	0.720	0.795	410	2610	370	2330	6.9		
1-8	13x4	0.405	0.545	530	3910	390	2880	11.8		
2-8	"	0.520	0.620	530	3560	420	2810	11.0	7.12	1.50
3-8	"	0.680	0.725	460	3250	390	2770	11.6		
4-8	"	0.835	0.905	390	2790	370	2560	9.9		
1-7	13x4	0.850	0.900	440	3430	420	3260	13.5	7.79	
1-6	"	0.755	0.885	320	2960	300	2790	5.7		
2-6		0.725	0.795	330	2900	290	2690	5.3	9.51	1.33
3-6	"	0.540	0.675	370	3370	310	2770	6.1		

Table 1 continued

Spec. No.	ℓxd	a_o	a_c	σ	τ_c	k_1	k_{2c}	t	τ_c/σ_c	n
2-0	4x11	0.650	0.790	0	3900	0	3470	5.2		
3-0	"	1.115	1.255	0	3430	0	3840	6.0		
4-0	"	.750	0.910	0	3850	0	3670	5.5		
5-0	"	1.010	1.200	0	3730	0	4080	4.4		
6-0	"	0.760	0.950	0	4290	0	4180	6.5		
8-0	"	1.050	1.180	0	3080	0	3350	3.7		
9-0	"	0.810	0.915	0	3670	0	3510	4.8		
10-0	"	0.520	0.620	0	4360	0	3430	5.8		
12-0	"	0.495	0.650	0	4390	0	3540	5.6	∞	1.05
13-0	"	0.285	0.425	0	5020	0	3270	7.5		
17-0	"	0.285	0.395	0	5250	0	3300	11.1		
18-0	"	0.620	0.690	0	4130	0	3420	5.6		
19-0	"	0.650	0.875	0	3830	0	3580	5.8		
20-0	"	0.615	0.790	0	4250	0	3770	5.9		
21-0	"	0.420	0.460	0	4580	0	3110	6.8		
22-0	"	0.470	0.645	0	4840	0	3890	6.6		
23-0	"	0.445	0.520	0	4680	0	3370	6.5		

Fig.1 SPECIMEN UNDER TENSION LOADING

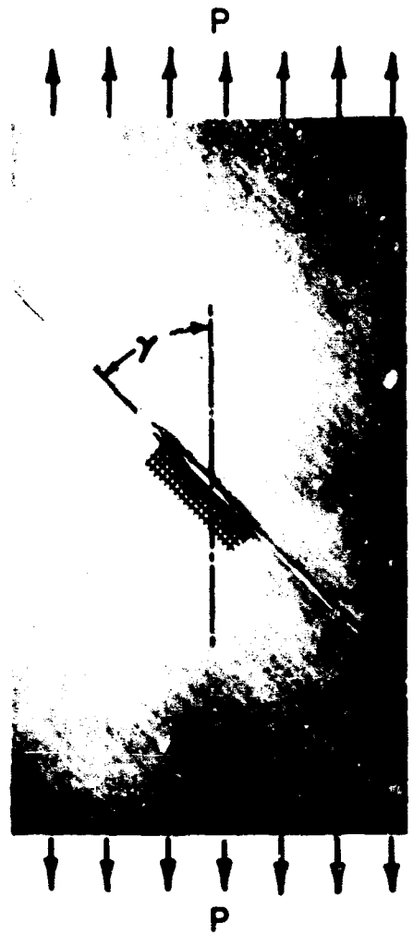

Fig. 2 SPECIMEN UNDER COMBINED TENSION AND SHEAR LOADING

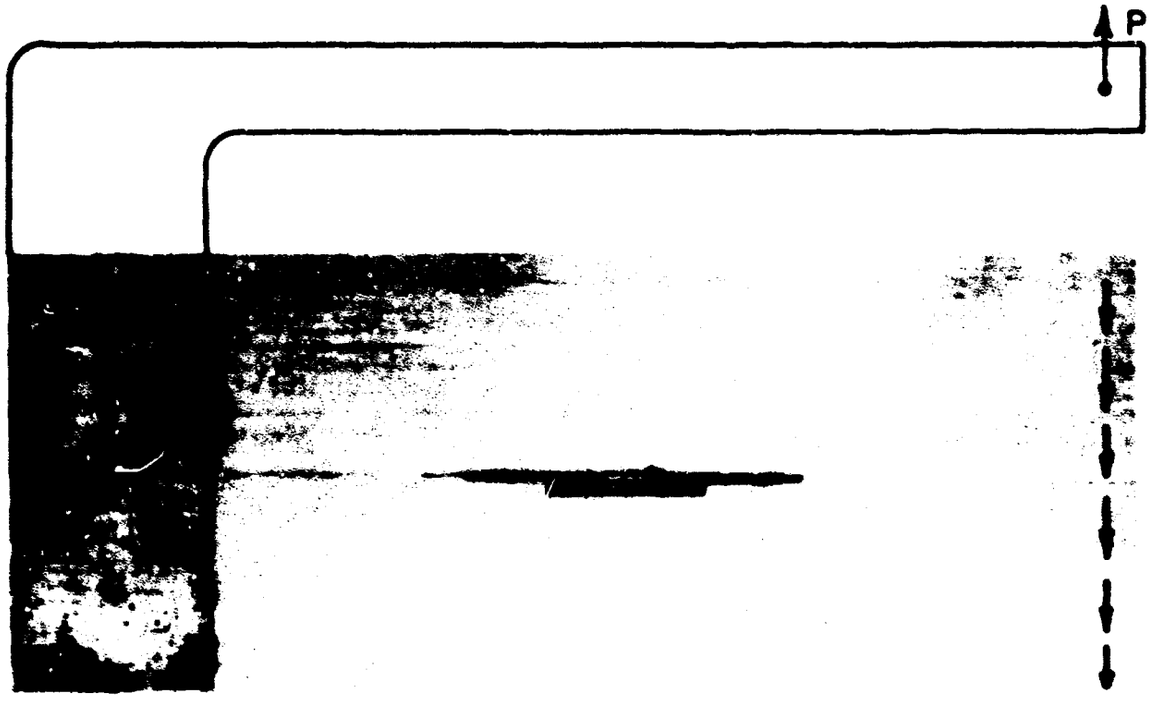

Fig. 3 SPECIMEN UNDER PURE SHEAR LOADING

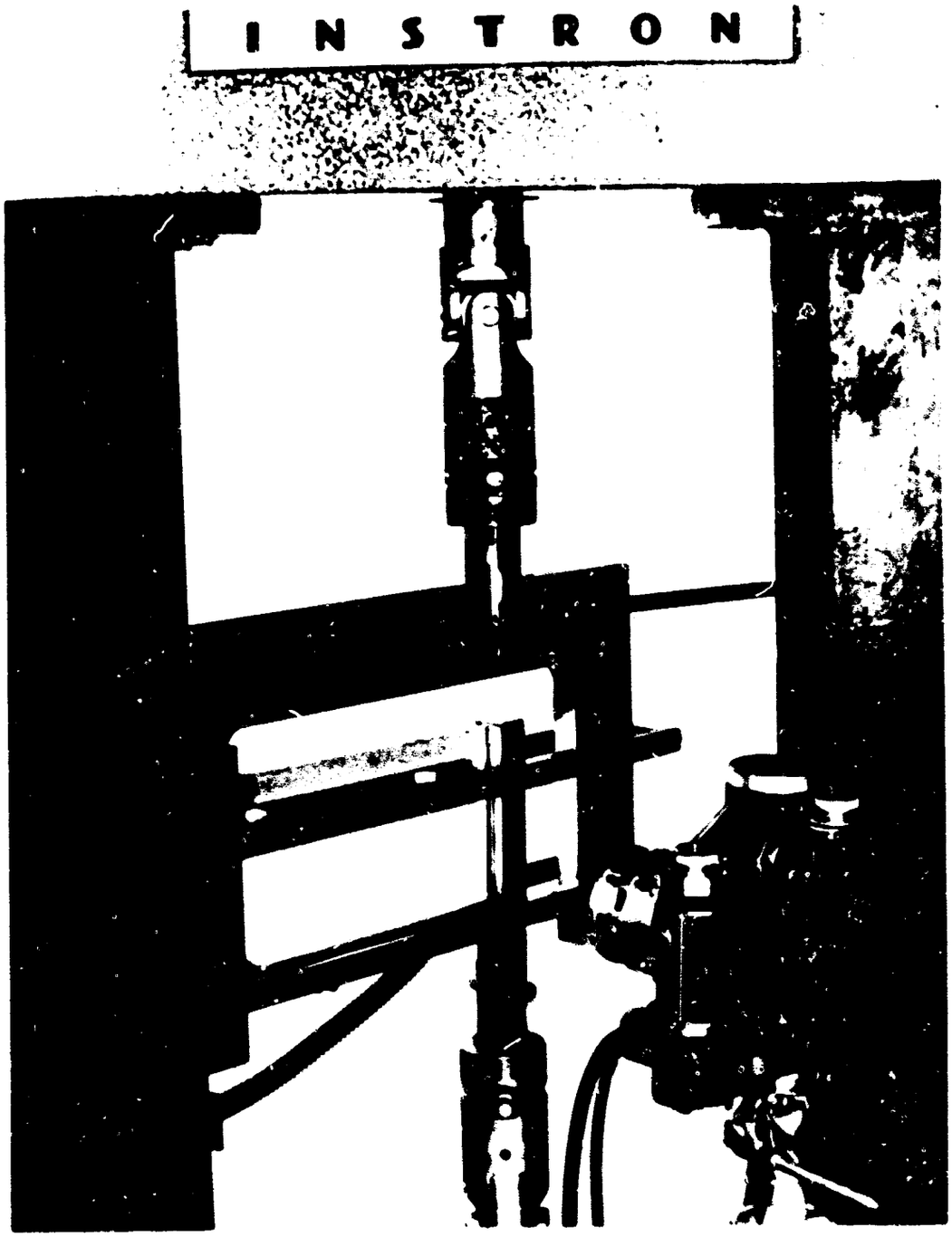

Fig. 4 APPARATUS USED TO OBTAIN PURE SHEAR

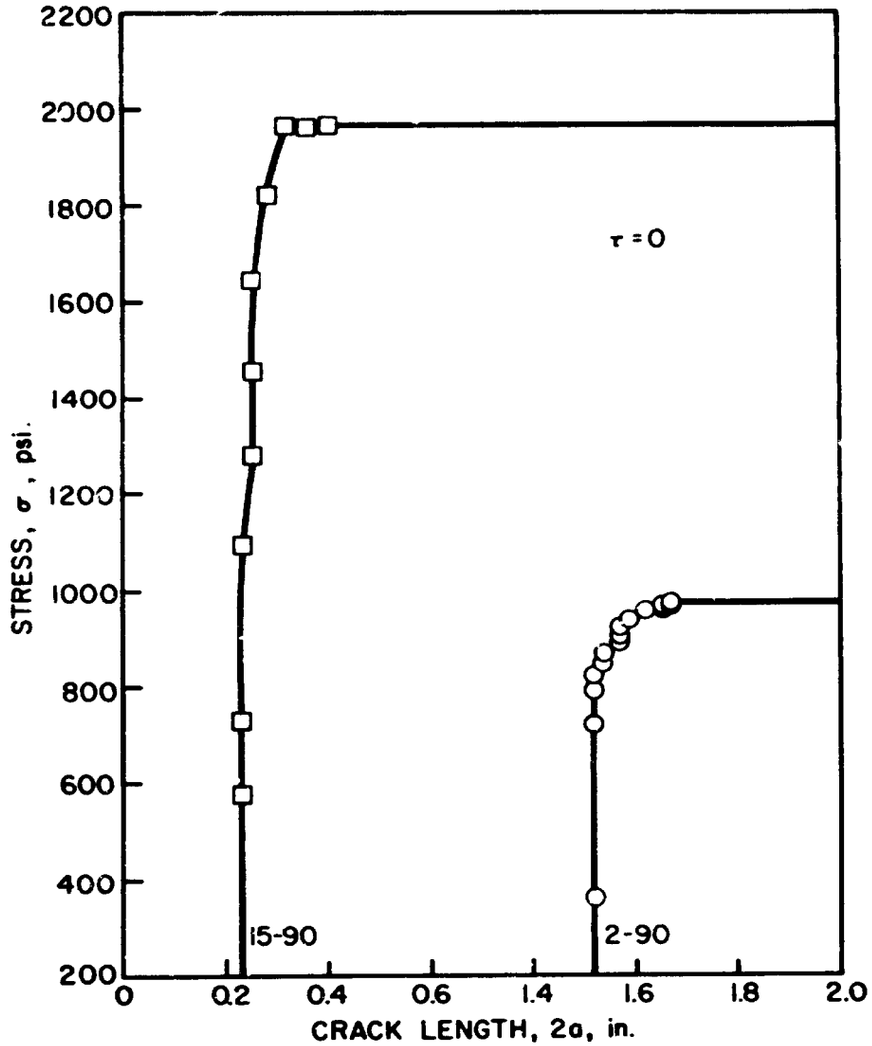

Fig. 5 TYPICAL CRACK EXTENSION PATTERNS OF SPECIMENS SUBJECTED TO TENSION

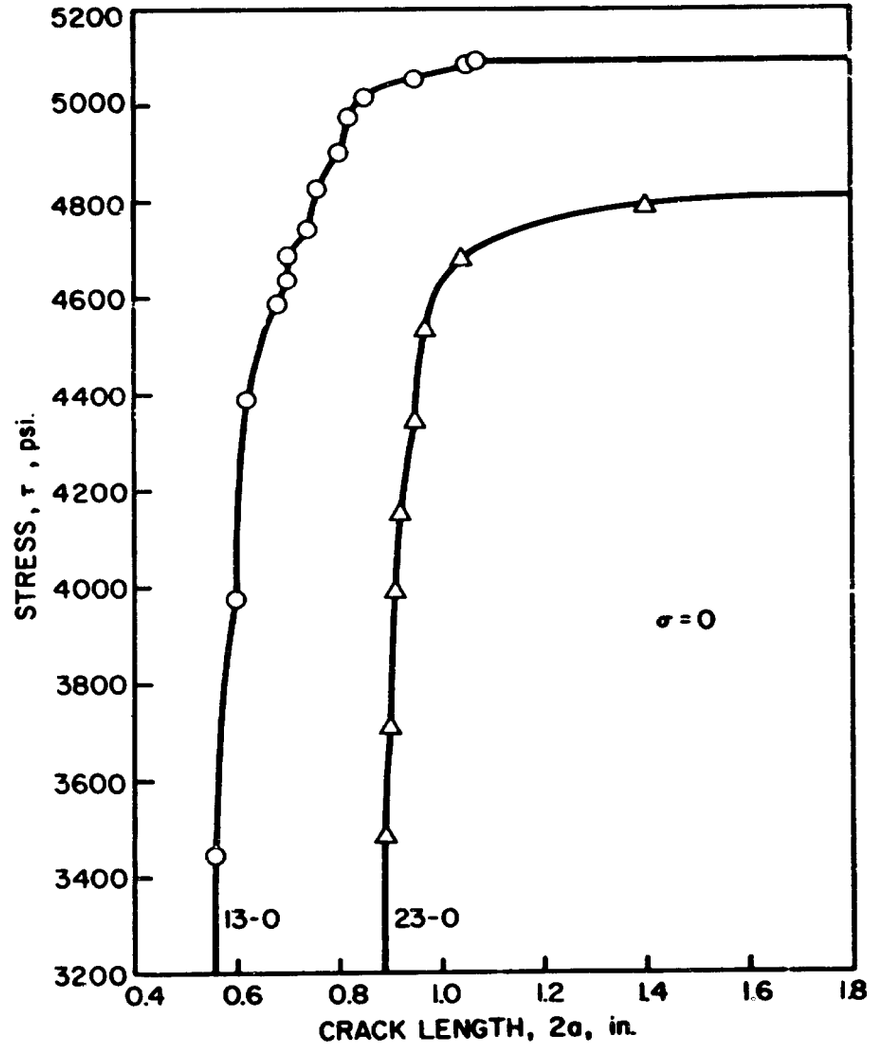

Fig. 6 TYPICAL CRACK EXTENSION PATTERNS OF SPECIMENS SUBJECTED TO PURE SHEAR

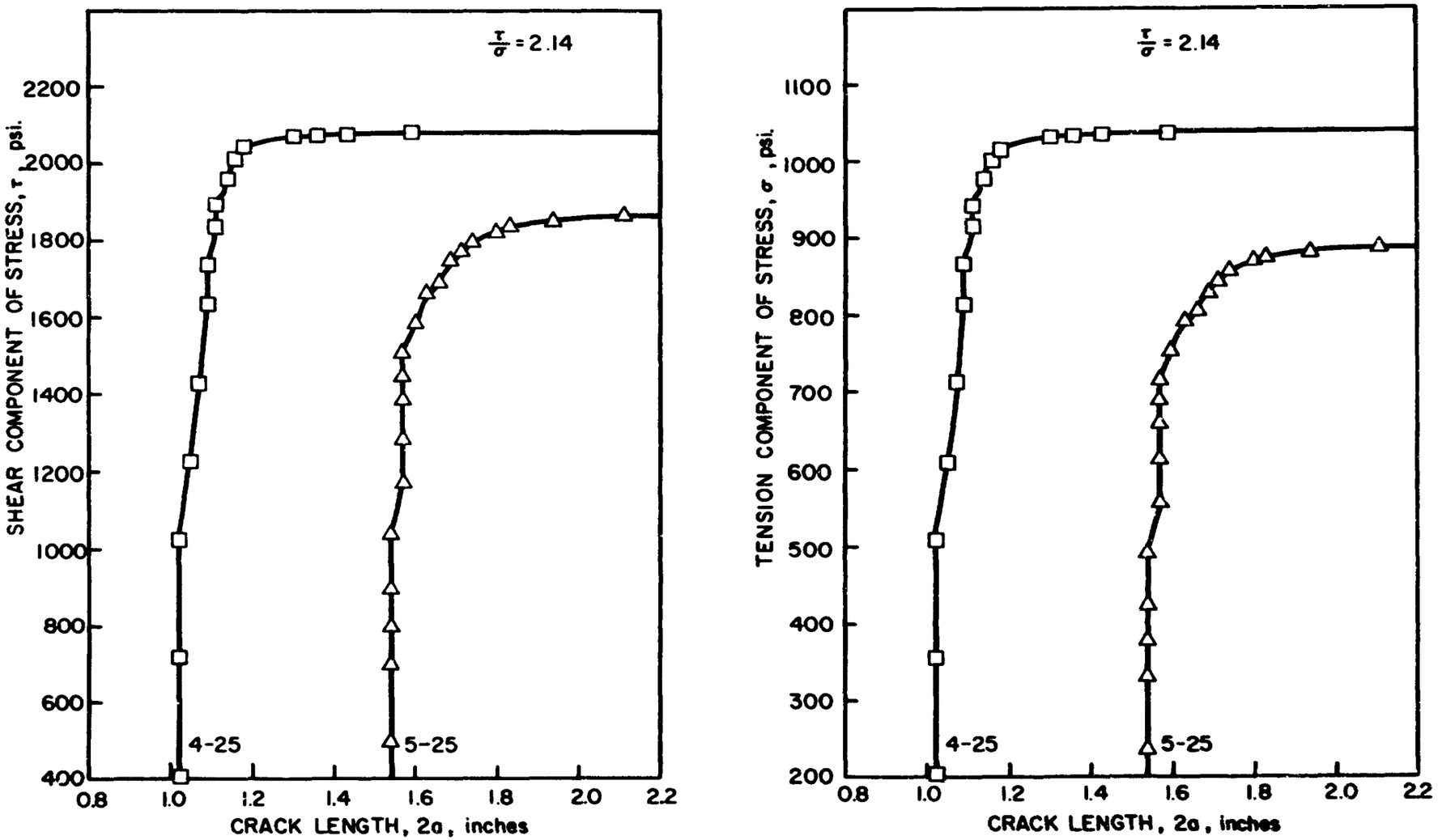

Fig. 7 TYPICAL CRACK EXTENSION PATTERNS OF SPECIMENS SUBJECTED TO COMBINED TENSION & SHEAR

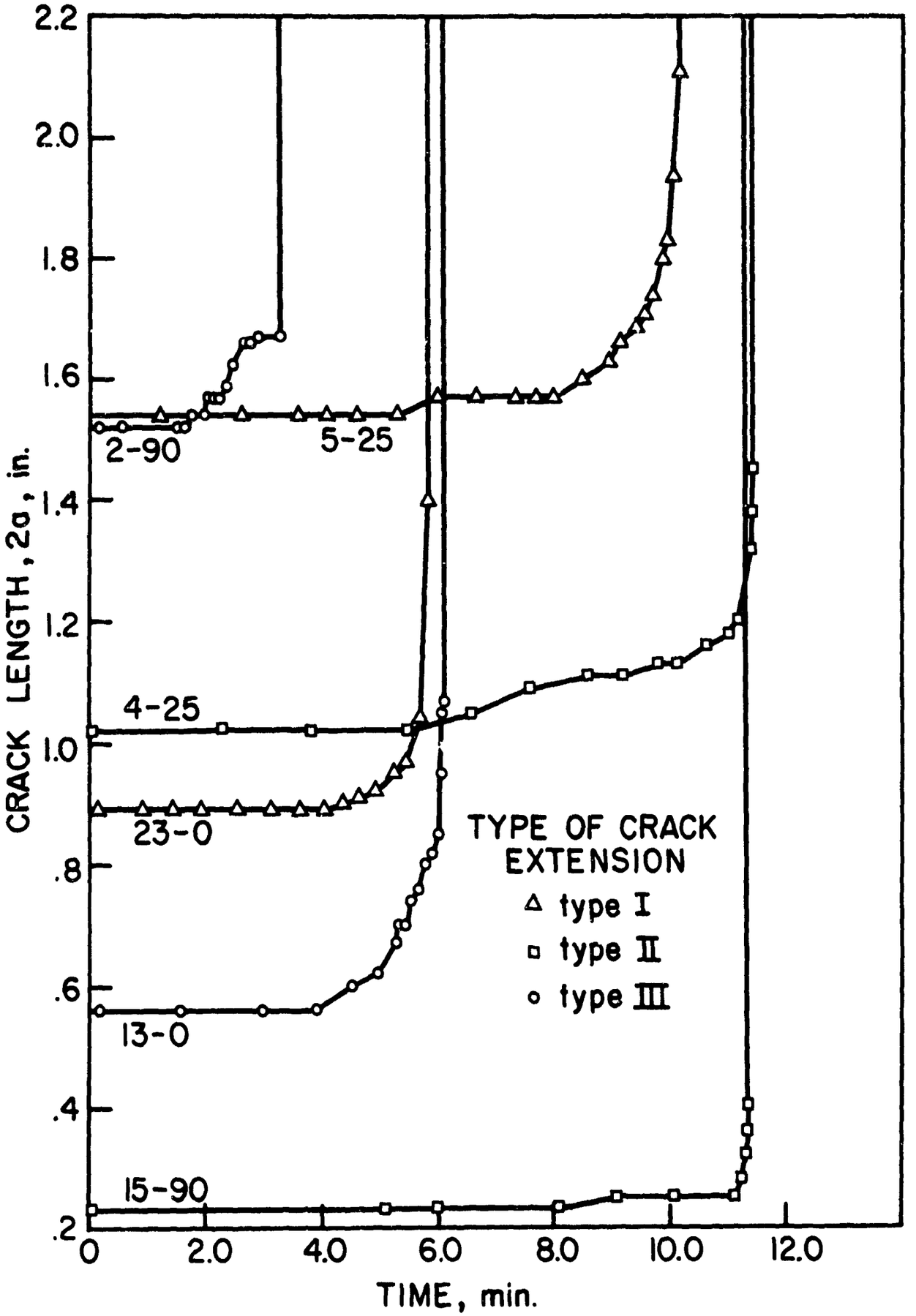

Fig. 8 TYPICAL CRACK EXTENSION-TIME CURVES

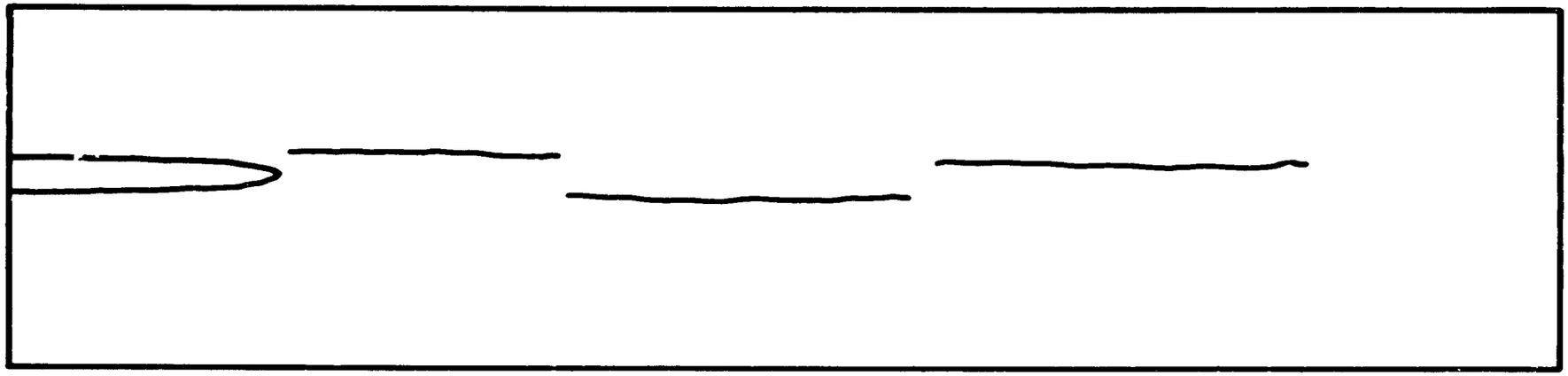

Fig. 9 SCHEMATIC OF A CRACK EXTENDED BY SKIPPING ACROSS FIBERS

Fig. 10 PHOTOGRAPH OF POORLY DEFINED CRACK TIP SHOWING MODE OF FIBER SKIPPING

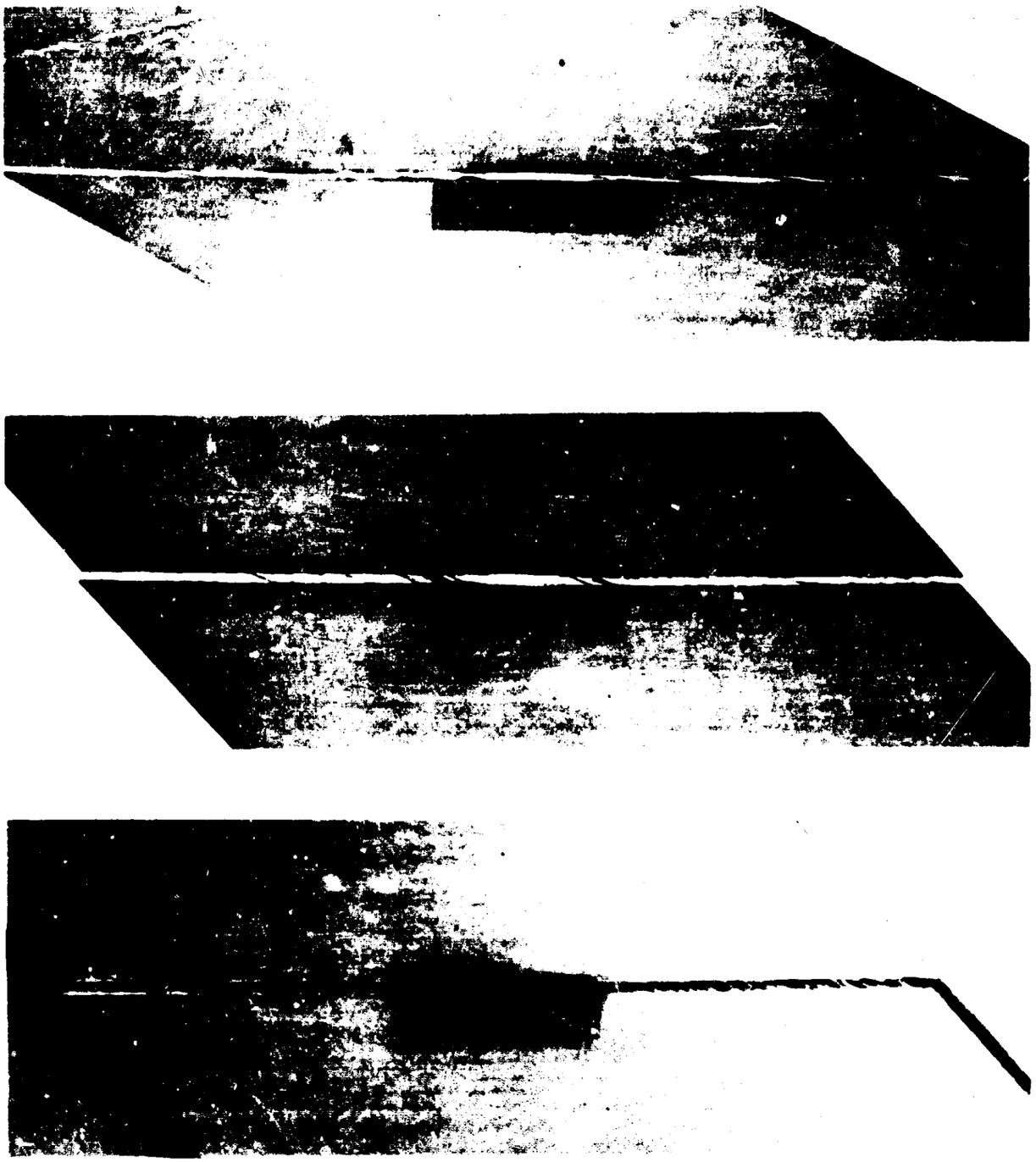

Fig. 11 BROKEN SPECIMENS IN WHICH THE CRACKS SKIPPED ACROSS FIBERS

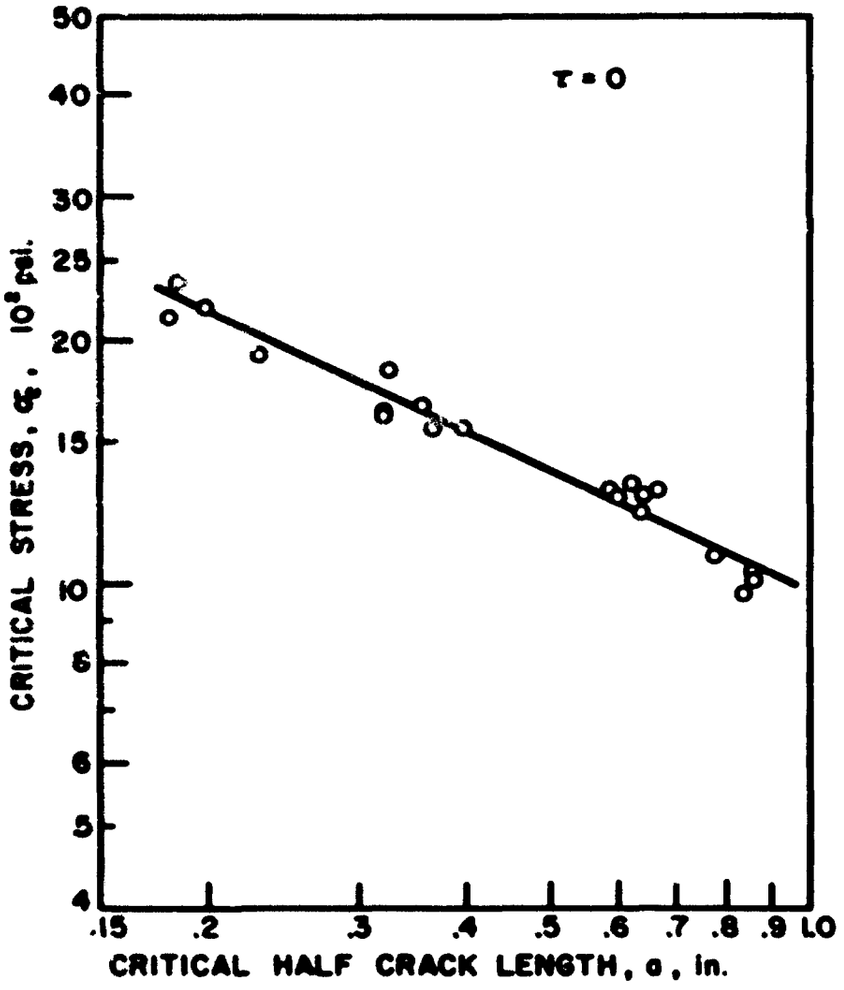

Fig. 12 RESULTS OF TENSION TESTS

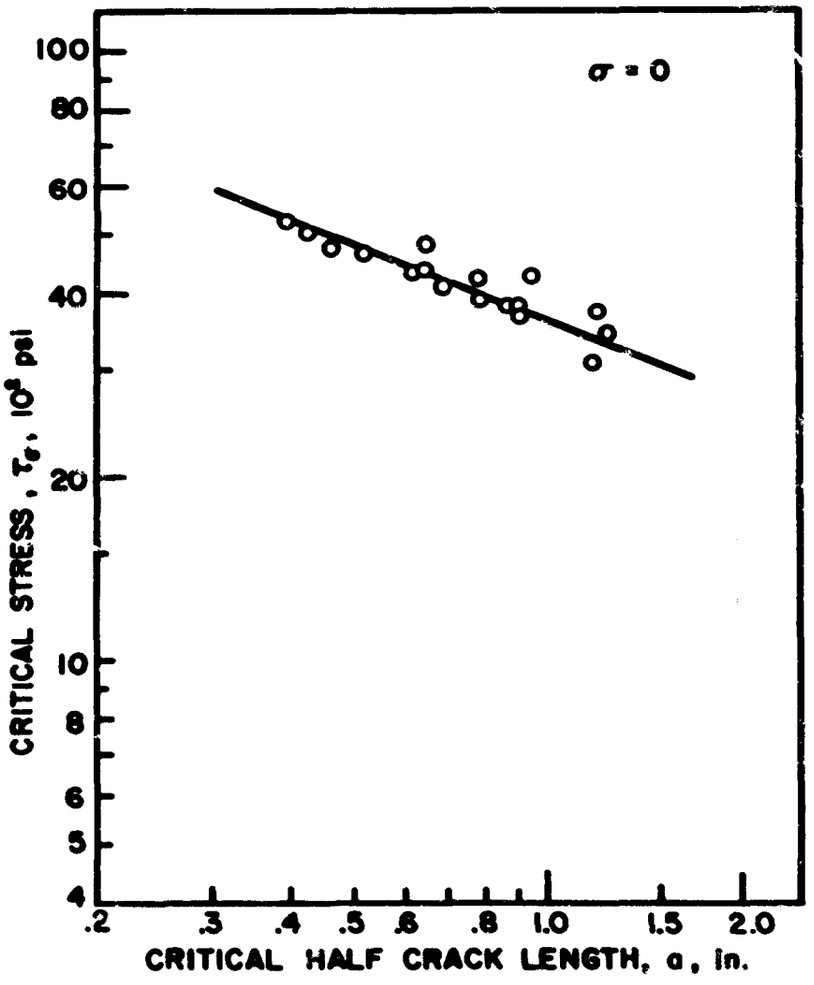

Fig. 13 RESULTS OF SHEAR TESTS

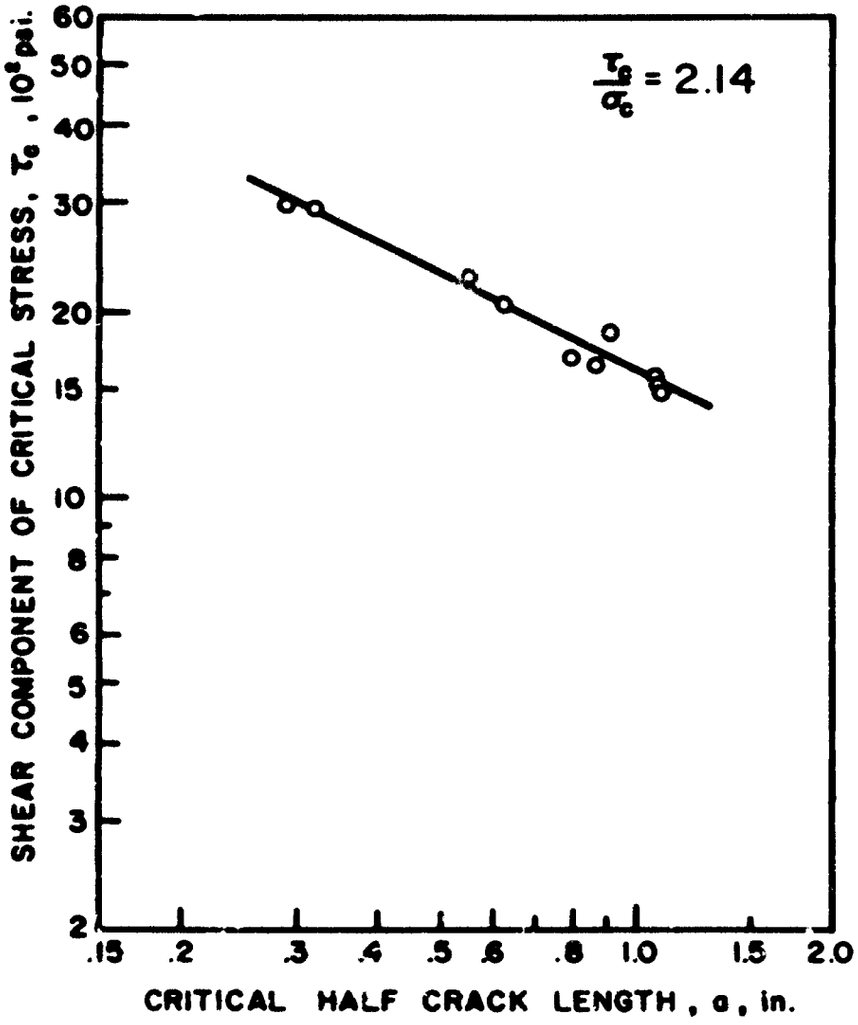

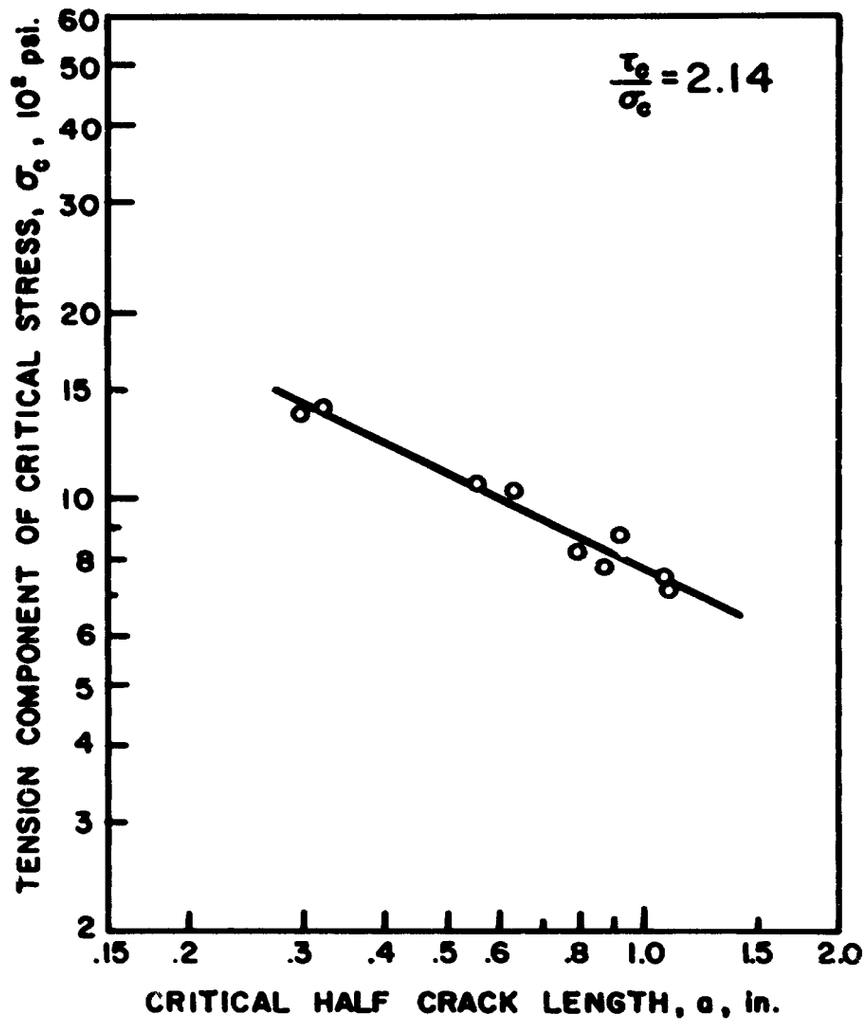

Fig. 14,15 RESULTS OF COMBINED TENSION AND SHEAR TESTS

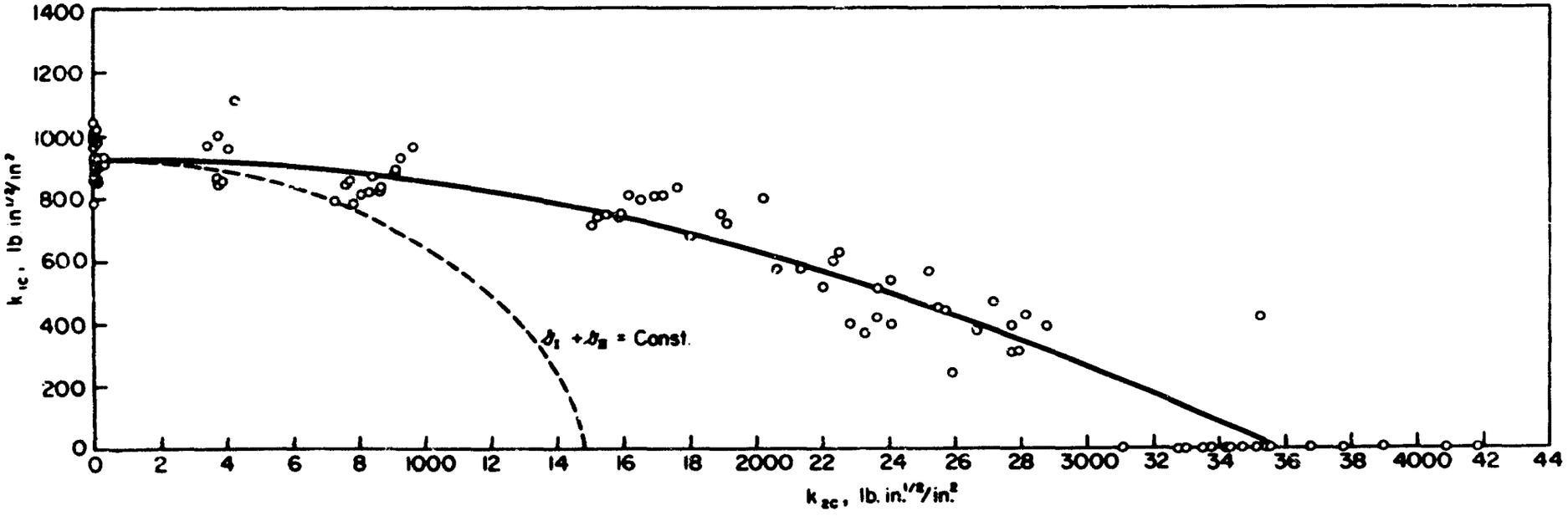

Fig. 16 INTERACTION BETWEEN CRITICAL SYMMETRIC STRESS INTENSITY FACTOR k_{1c} AND CRITICAL SKEW-SYMMETRIC STRESS INTENSITY FACTOR k_{2c} FOR SCOTCH-PLY

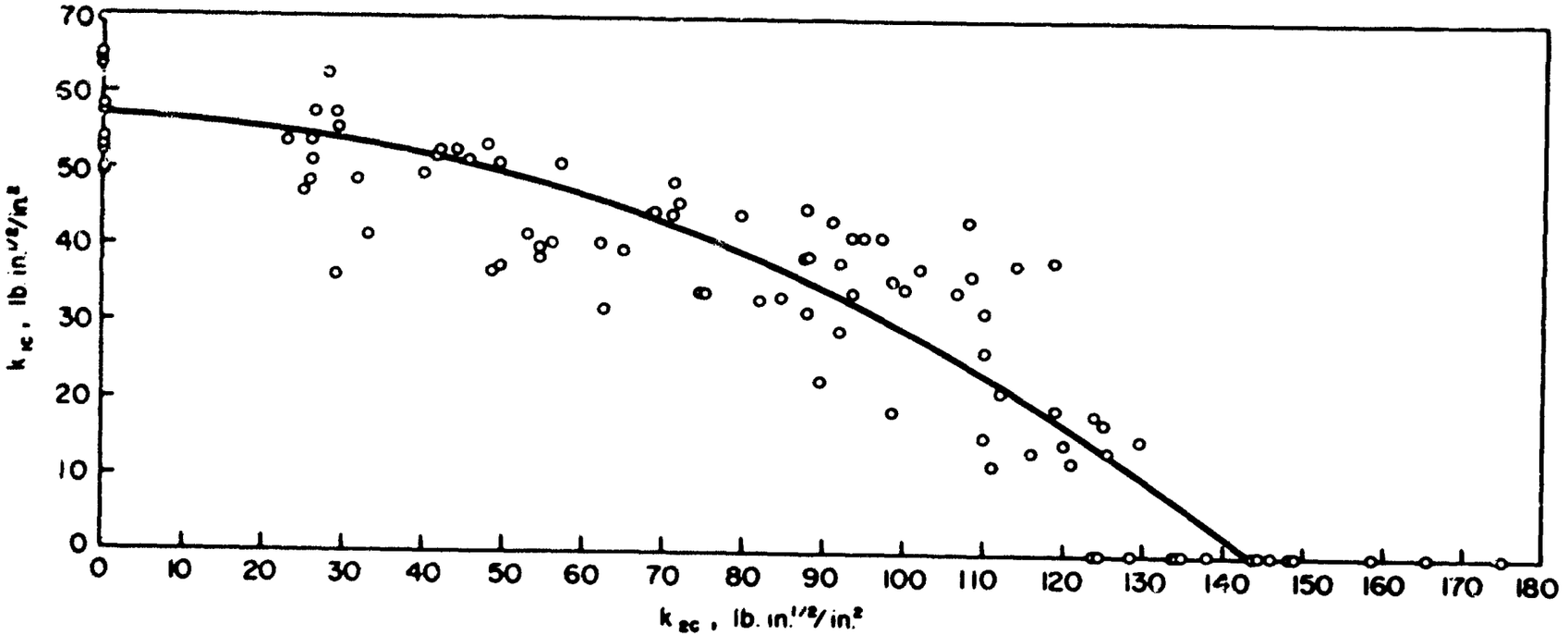

Fig. 17 INTERACTION BETWEEN CRITICAL SYMMETRIC STRESS INTENSITY FACTOR k_{ic} AND CRITICAL SKEW-SYMMETRIC STRESS INTENSITY FACTOR k_{2c} FOR BALSA WOOD

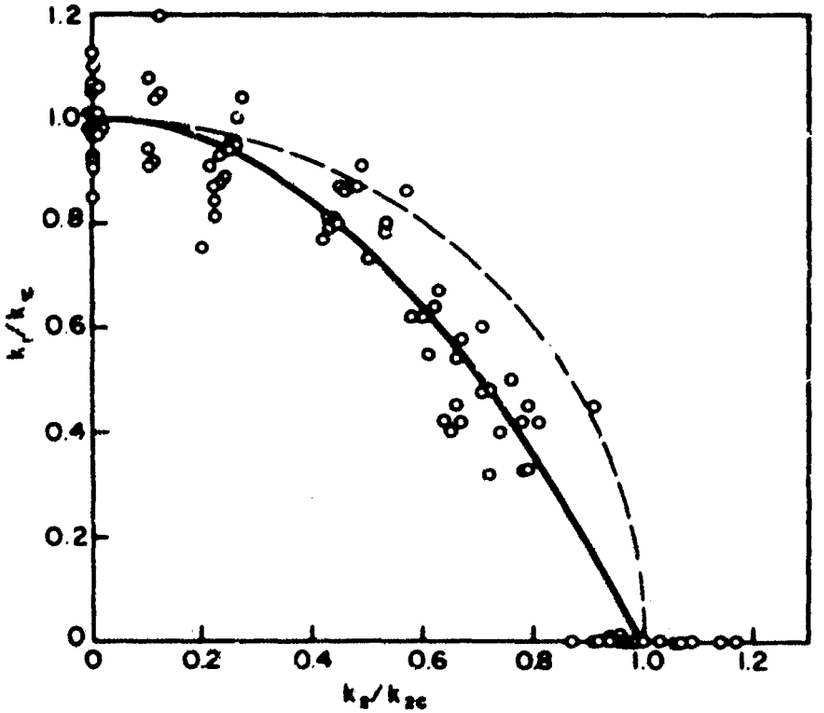

Fig. 18 DIMENSIONLESS REPRESENTATION OF INTERACTION BETWEEN STRESS INTENSITY FACTORS k_{1c} AND k_{2c} FOR SCOTCH-PLY

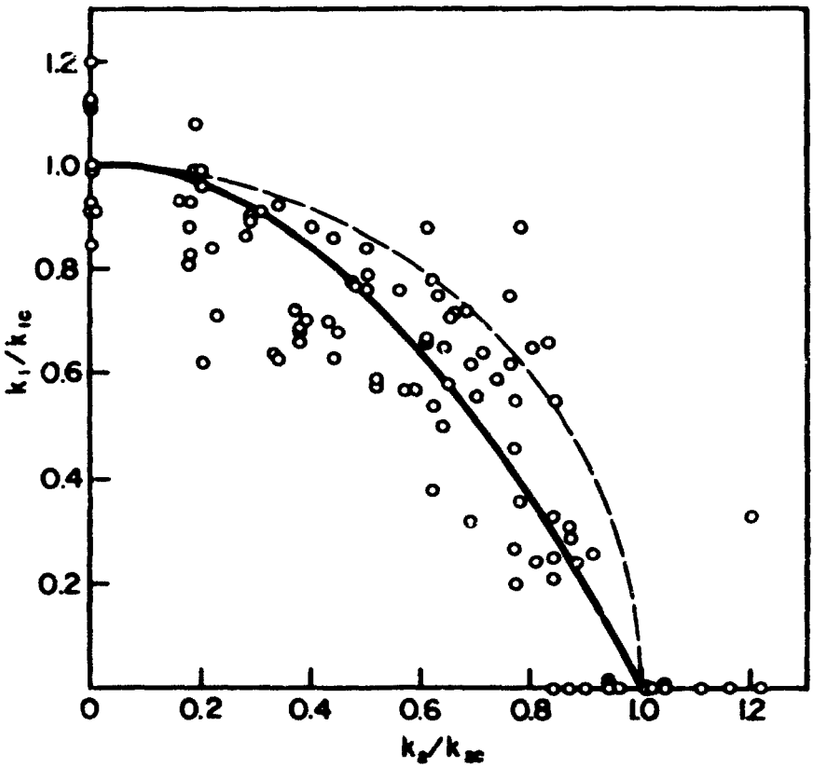

Fig. 19 DIMENSIONLESS REPRESENTATION OF INTERACTION BETWEEN STRESS INTENSITY FACTORS k_{1c} AND k_{2c} FOR BALSA WOOD